ACADEMIC PRESS

Available online at www.sciencedirect.com
SCIENCE DIRECT®

Journal of Catalysis 218 (2003) 123–134

JOURNAL OF CATALYSIS

www.elsevier.com/locate/jcat

Thermolytic molecular precursor routes to Cr/Si/Al/O and Cr/Si/Zr/O catalysts for the oxidative dehydrogenation and dehydrogenation of propane

Kyle L. Fujdala and T. Don Tilley *

Department of Chemistry, University of California, Berkeley, Berkeley, CA 94720-1460, USA
Chemical Sciences Division, Lawrence Berkeley National Laboratory, 1 Cyclotron Road, Berkeley, CA 94720-1460, USA

Received 29 October 2002; revised 10 March 2003; accepted 14 March 2003

Abstract

Cothermolyses of $(^tBuO)_3CrOSi(O^tBu)_3$ (**1**) and either $[Al(O^tBu)_3]_2$ (**2**) or $Zr[OCMe_2Et]_4$ (**3**) as solutions in *n*-octane resulted in formation of gels that yielded Cr/Si/Al/O or Cr/Si/Zr/O xerogels upon drying. These materials have high surface areas after calcination at 773 K (ranging from 150 to 450 $m^2\,g^{-1}$) and do not exhibit phase separation of Cr_2O_3 domains after calcination at 1473 K (by PXRD). The as-synthesized Cr/Si/M materials contain mostly octahedral Cr^{3+} species with small amounts of tetrahedral Cr^{6+} chromates (by DRUV–vis and XANES spectroscopies). Only Cr^{6+} monochromate centers, with smaller amounts of di- and polychromate species, were detected after calcination at 773 K under O_2. These catalysts are active for the oxidative dehydrogenation (ODH) of propane; however, they exhibit poor selectivities for propylene production. In contrast, these catalysts exhibit high selectivities for propylene (> 95%) in the nonoxidative dehydrogenation (DH) of propane with conversions for the best catalyst above 35% at 723 K.

Keywords: Molecular precursor; Cothermolysis; Propane oxidative dehydrogenation; Propane dehydrogenation; Chromium; Oxide catalyst

1. Introduction

An important goal in the synthesis of new heterogeneous catalysts is the generation of materials containing well-dispersed catalytic centers within a support matrix. Additionally, efficient catalysts should be highly homogeneous to ensure uniformity in properties. Significantly, multicomponent oxide materials with isolated (well-dispersed) catalytic centers are often metastable, requiring use of low-temperature synthetic procedures that provide a degree of atomic-level control over the resulting active sites [1–14]. The sol–gel process has been widely employed for the low-temperature preparation of oxide materials [1–14]. While this method has proven quite successful for the preparation of relatively simple oxide materials, it is not generally suitable for generating homogeneous binary and higher order multicomponent oxides due to the different rates of hydrolysis for each sol–gel precursor. Although this problem can be controlled to some extent by careful modification of the precursor structure, or by the prehydrolysis of one precursor prior to addition of a second, use of this process for the construction of homogeneous multicomponent oxides is still rather limited [1–14]. Alternative low-temperature methods for the synthesis of complex heteroelement oxides are required for the production of highly homogeneous and potentially more efficient catalytic materials.

In developing new routes to homogeneous materials, we have investigated the structure, bonding, and reactivity of tris(*tert*-butoxy)siloxy complexes of the form $L_nM[OSi(O^tBu)_3]_x$ [15–26]. These oxygen-rich compounds serve as convenient molecular precursors to carbon-free, homogeneous M/Si/O materials in low-temperature thermolytic conversions (typically below 473 K), via the elimination of isobutylene and water. Solution thermolyses of these precursors in nonpolar media (toluene, *n*-octane, etc.) give rise to gels that ultimately form high surface area xerogels upon conventional drying. This *thermolytic molecular precursor* (TMP) route to multicomponent oxides has been utilized for the production of a variety of homogeneous metal-

* Corresponding author.
E-mail address: tdtilley@socrates.berkeley.edu (T.D. Tilley).

0021-9517/03/$ – see front matter
doi:10.1016/S0021-9517(03)00141-6

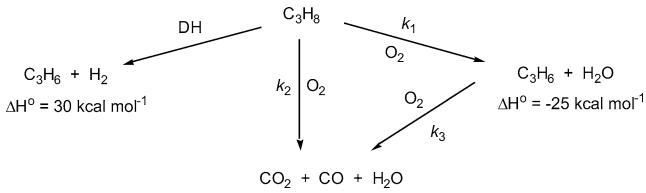

Scheme 1.

silicon-oxide materials with tailored properties [15–26]. The TMP method offers several advantages over traditional synthetic procedures for catalyst syntheses. These include use of well-defined species for control over the stoichiometry, the preexistence of M–O–E linkages to maximize the homogeneity, and the use of nonpolar solvents to reduce pore collapse upon drying. Other groups have also developed nonaqueous routes to oxide materials, including the condensation of metal alkoxides with metal acetates [27] or metal halides [28].

We have recently extended the TMP method to the cothermolysis of precursor complexes [29,30]. This cothermolytic method has allowed the syntheses of catalytic V/Si/Zr/O and V/Zr/O materials via thermolyses of solutions containing $OV[OSi(O^tBu)_3]_3$ and $Zr[OCMe_2Et]_4$, or $OV(O^tBu)_3$ and $Zr[OCMe_2Et]_4$, respectively. By altering the ratio of precursors, this method allows the synthesis of high surface area, uniform materials with a wide range of predetermined compositions [29,30].

The conversion of propane to propylene is an important industrial process, and the demand for propylene is rapidly increasing given its use in the production of propylene oxide, acrylonitrile, and polypropylene [31–47]. Currently, propylene is primarily produced by the high temperature cracking of hydrocarbons; however, the controlled dehydrogenation of propane provides a useful alternative process [31–47] (Scheme 1). The endothermic dehydrogenation (DH) of propane, currently employed on an industrial scale, utilizes Cr-based catalysts with Al_2O_3 as a support and alkali metal promoters [32]. Unfortunately, these propane DH reactions require high temperatures (up to 873 K) which lead to cracking and the deposition of carbon. This reduces the overall efficiency of the catalysis and requires a catalyst regeneration step [32–47]. In studies on various chromium-based catalysts, DeRossi and co-workers found that Cr/ZrO_2 catalysts exhibited increased activity over similarly prepared Cr/Al_2O_3 and Cr/SiO_2 materials [42–45]. However, it was also concluded that the practical use of these Cr/ZrO_2 catalysts would require an increase in their surface areas and greater thermal stability under the reaction conditions [42].

The oxidative dehydrogenation (ODH) of propane represents an alternative synthesis for propylene that can be performed at lower temperatures and does not suffer from coking [31,33,38,39,48–51]. However, the tendency of the propylene product to overoxidize is a significant obstacle for the commercialization of this process, and therefore the development of more efficient catalysts is highly desired. Many of the best propane ODH catalysts are based on vanadium [48–51], and TMP-derived V/Zr/O catalysts perform at levels among the very best of these [29,30]. A recent report claims that Cr/Al_2O_3 catalysts are moderately active and selective for propane ODH, although their performance was below that of many vanadium-based catalysts [33].

Given the reported efficiency of Cr-based dehydrogenation catalysts, it was of interest to utilize the TMP cothermolysis method for the generation of such materials with high surface areas and highly dispersed active sites. We previously reported synthesis of the molecular precursor $(^tBuO)_3CrOSi(O^tBu)_3$ (**1**) and demonstrated its efficient conversion to high surface area (300 $m^2\,g^{-1}$) Cr/Si/O materials via TMP methods [23]. Herein, we describe the use of **1** for the generation of high surface area Cr/Si/Al/O and Cr/Si/Zr/O catalytic materials via cothermolyses with $[Al(O^tBu)_3]_2$ (**2**) or $Zr[OCMe_2Et]_4$ (**3**) in a nonpolar solvent. The efficiency of these materials for the dehydrogenation of propane was tested under oxidative (ODH) and non-oxidative (DH) conditions, and the results of these investigations are presented here.

2. Experimental details

2.1. General

All synthetic manipulations were performed under an atmosphere of N_2 using standard Schlenk techniques and/or a Vacuum Atmospheres drybox, unless noted otherwise. Solvents were distilled from sodium/benzophenone, potassium/benzophenone, sodium, or calcium hydride, as appropriate. Thermal analyses were performed using a TA Instruments SDT 2960 integrated thermogravimetric/differential thermal analyzer (TGA/DTA) with a heating rate of 10 K min^{-1} under N_2 or O_2, as appropriate. N_2 porosimetry measurements were performed using a Quantachrome Autosorb surface area analyzer with samples heated at 393 K, under reduced pressure, for a minimum of 4 h immediately prior to data collection. PXRD data were collected using a Siemens D5000 diffractometer operating with θ–2θ geometry at room temperature (Cu-K_α radiation, 1.5 s collection time, and 0.02° step size). DRUV–vis spectra were acquired using a Perkin-Elmer Lambda-9 spectrophotometer equipped with a 60-mm integrating sphere (ratio of apertures to sphere surface $= \sim 8\%$), a slit width of 4 nm, and a collection speed of 120 nm min^{-1}. Samples were run without dilution in equal quantities (10 mg each) using $BaSO_4$ as a reference material. XAS measurements were performed at the Stanford Synchrotron Radiation Laboratory (SSRL) using beamline 2-3. X-ray detection was performed in transmission mode using a Si (111) double crystal monochromator and two ion chambers. Data were collected at 298 K on dried samples sealed under an atmosphere of N_2 and diluted with BN. The XANES data were analyzed using WinXas 97 software. TEM images were recorded using a JEOL 200cx transmission electron microscope operating at

200 kV. Samples for TEM analysis were prepared by deposition using a pentane suspension of finely ground material on a "Type A" carbon-coated copper grid obtained from Ted Pella, Inc. Elemental analyses were performed by Galbraith Laboratories (Knoxville, TN). $(^t\mathrm{BuO})_3\mathrm{CrOSi}(\mathrm{O}^t\mathrm{Bu})_3$ (**1**) was prepared as previously reported [23], $[\mathrm{Al}(\mathrm{O}^t\mathrm{Bu})_3]_2$ (**2**) was purchased from Aldrich and purified by sublimation, and $\mathrm{Zr}[\mathrm{OCMe_2Et}]_4$ (**3**) was purchased from Gelest and purified by distillation.

2.2. Syntheses of Cr/Si/M/O xerogels

A representative ***n*CrSiAl** xerogel preparation: A solution of **1** (0.107 g, 0.2 mmol) and **2** (0.443 g, 1.8 mmol) in *n*-octane (5.0 mL) was sealed in a thick-walled Pyrex pyrolysis tube after three freeze-pump-thaw cycles. The tube was then placed in a preheated oven (453 K) for 48 h. The light green monolithic gel that resulted was washed with *n*-octane (3 mL), air dried for 2 days at 298 K, and dried in vacuo at 398 K for 12 h yielding a xerogel (**10CrSiAl**). Xerogel calcinations were performed in a Lindberg 1473 K three-zone tube furnace under flowing O_2 ($100\ \mathrm{mL\,min^{-1}}$) with a heating rate of $10\ \mathrm{K\,min^{-1}}$ and a 2 h isothermal stage at the final temperature. For other ***n*CrSiAl** samples, amounts of **1** and **2** were varied such that the total concentration of the solution was maintained at 0.4 M. The ***n*CrSiZr** xerogels were prepared using solutions of **1** and **3** in *n*-octane (4 M) in an analogous fashion. For the preparation of pure Al_2O_3 and ZrO_2 samples, solutions of **2** or **3** in *n*-octane (0.4 M) were treated as above except that the solution of **3** was heated at 498 K to facilitate thermolysis.

2.3. Catalytic dehydrogenation of propane

Selectivities and conversions for the propane to propylene reactions were measured using a fixed-bed flow reactor (quartz) fitted with a medium frit. Quartz chips (0.500 g, 0.246–0.494 mm) were used to disperse each catalyst within the reactor. The mass of catalyst used varied between 0.010 and 0.260 g as noted in Tables 3–5. The gas stream for the ODH reactions consisted of helium (typically 200 $\mathrm{mL\,min^{-1}}$), propane (25 $\mathrm{mL\,min^{-1}}$), nitrogen (2 $\mathrm{mL\,min^{-1}}$), and oxygen (9 $\mathrm{mL\,min^{-1}}$). Propane and oxygen conversions were varied by changing the total flow rate (between 40 and 240 $\mathrm{mL\,min^{-1}}$). Typical DH reactions used a gas stream consisting of helium ($\sim 32\ \mathrm{mL\,min^{-1}}$), propane ($\sim 2\ \mathrm{mL\,min^{-1}}$), and nitrogen (10% of the propane flow). Dilution was achieved by increasing the amount of He and residence times were varied via changes in the total flow rate. For ODH reactions, the catalysts were calcined at 773 K under $\mathrm{He/O_2}$ ($\sim 10/1$; $\sim 200\ \mathrm{mL\,min^{-1}}$) for 2 h prior to reaction. For DH reactions, the catalysts were calcined at 773 K for 2 h under $\mathrm{He/O_2}$ ($\sim 10/1$; $\sim 200\ \mathrm{mL\,min^{-1}}$), and subsequently for 2 h under He ($\sim 200\ \mathrm{mL\,min^{-1}}$). For ODH and DH reactions, the gaseous reactants and products were analyzed online using a Hewlett-Packard 6890 gas chromatograph equipped with both a capillary column (HP-1) and a packed column (HAYESEP-Q). C_3H_6, CO, CO_2, and H_2O were detected as the ODH reaction products and CH_4, C_2H_4, C_2H_6, and C_3H_6 were the DH reaction products detected after ~ 30 min of reaction time. Immediately after catalyst exposure to propane under DH conditions, some CO_x species were detected, presumably due to initial ODH activity upon reduction of the Cr^{6+} species [32]. After ~ 30 min of reaction time no further CO_2 was observed under DH conditions; however, small amounts of CO were observed throughout ($< 1\%$), presumably as a result of partial oxidation by lattice oxygen. The ODH reactions were run at 606 and 673 K while the DH reactions were run at 723 or 763 K. Typical propane conversions ranged from ~ 1 to 10% for the ODH reactions and from ~ 0.5 to 38% for the DH reactions. Oxygen conversions in the ODH reactions ranged from 1 to 15% at 606 K and from 11 to 69% at 673 K.

3. Results and discussion

3.1. Thermolytic molecular precursor route to Cr/Si/M/O xerogels

Thermolyses of *n*-octane solutions containing $(^t\mathrm{BuO})_3\mathrm{CrOSi}(\mathrm{O}^t\mathrm{Bu})_3$ (**1**) and either $[\mathrm{Al}(\mathrm{O}^t\mathrm{Bu})_3]_2$ (**2**) or $\mathrm{Zr}[\mathrm{OCMe_2Et}]_4$ (**3**) at 453 K resulted in the formation of gelatinous precipitates that, upon drying in air, formed xerogels [***n*CrSiAl** and ***n*CrSiZr**, where n = mol% of **1** used versus **2** or **3**; Eqs. (1) and (2)]. The independent solution thermolyses of **2** and **3** (at 453 and 498 K, respectively) gave gels that, upon drying, provided Al_2O_3 and ZrO_2 xerogels. Note that the thermal decomposition of **3** occurs at a lower temperature upon cothermolysis with **1**, suggesting that **1** or its decomposition products catalyze the conversion of **3**. Similar behavior was observed for cothermolyses of **3** with $\mathrm{OV}[\mathrm{OSi}(\mathrm{O}^t\mathrm{Bu})_3]_3$ or $\mathrm{OV}(\mathrm{O}^t\mathrm{Bu})_3$ [29,30]. Xerogels were synthesized with 2.5 (**2.5CrSiAl** and **2.5CrSiZr**), 5 (**5CrSiAl** and **5CrSiZr**), and 10 (**10CrSiAl** and **10CrSiZr**) mol% of **1** (Table 1).

$$(^t\mathrm{BuO})_3\mathrm{CrOSi}(\mathrm{O}^t\mathrm{Bu})_3\ (\mathbf{1}) + [\mathrm{Al}(\mathrm{O}^t\mathrm{Bu})_3]_2\ (\mathbf{2}) \xrightarrow{453\ \mathrm{K,\ toluene}} \boldsymbol{n}\mathbf{CrSiAl}, \quad (1)$$

where $n = 2.5$, 5, and 10 mol% **1**.

$$(^t\mathrm{BuO})_3\mathrm{CrOSi}(\mathrm{O}^t\mathrm{Bu})_3\ (\mathbf{1}) + \mathrm{Zr}[\mathrm{OCMe_2Et}]_4\ (\mathbf{3}) \xrightarrow{453\ \mathrm{K,\ toluene}} \boldsymbol{n}\mathbf{CrSiZr}, \quad (2)$$

where $n = 2.5$, 5, and 10 mol% **1**.

The gels were dried at room temperature in air to give xerogels as pale-green powders. The as-synthesized Al_2O_3 and ZrO_2 xerogels from **2** and **3** were colorless powders. Calcination of the Cr/Si/M/O xerogels under O_2 ($100\ \mathrm{mL\,min^{-1}}$) at 773 K resulted in materials that maintained visual homogeneity with colors ranging from light to

Table 1
Properties of the xerogels after calcination at 773 K

Sample	Cr/Al or Cr/Zr molar ratio	Cr content (wt%)	Cr site density ($Cr\,nm^{-2}$)	Surface area ($m^2\,g^{-1}$)[a]	Pore volume ($cm^3\,g^{-1}$)	Average pore radius[b] (Å)
2.5CrSiAl	1:40	2.4	0.6	455	1.30	57.4
5CrSiAl	1:20	4.5	1.4	380	0.66	34.6
10CrSiAl	1:10	8.1	2.2	430	0.76	35.4
Al_2O_3	N/A	N/A	N/A	235	1.09	93.6
2.5CrSiZr	1:40	1.0	0.6	180	0.12	13.9
5CrSiZr	1:20	2.0	1.1	220	0.14	12.9
10CrSiZr	1:10	3.8	2.9	150	0.09	12.6
ZrO_2	N/A	N/A	N/A	90	0.21	47.6

[a] Rounded to the nearest 5 $m^2\,g^{-1}$ to reflect the error in measurement.
[b] Calculated from the 2(pore volume)/(area) method, assuming spherical particles.

dark yellow, depending on the Cr content. The Zr-containing materials were slightly darker in color than the corresponding Al-containing ones. The pure Al_2O_3 and ZrO_2 xerogels maintained their colorless (white) nature after calcination at 773 K in O_2.

3.2. Characterization of the xerogels

Nitrogen porosimetry was used to determine the surface areas and pore volumes of the ***n*CrSiAl** and ***n*CrSiZr** xerogels. The Brunnaur–Emmett–Teller (BET) method [52] was used to calculate the surface areas and the Barrett–Joyner–Halenda (BJH) method was used to obtain the pore size distributions [53]. Table 1 provides a summary of the nitrogen porosimetry data for all of the xerogels after calcination at 773 K. The presence of **1** in the thermolysis mixture gives rise to an increase in the surface area of the resulting xerogels relative to those of the pure Al_2O_3 and ZrO_2 xerogels obtained from **2** and **3**, respectively. This effect is undoubtedly due to the presence of Si (and possibly Cr); however, the surface areas do not correlate proportionately with the amount of **1** present [18,21–26]. Also, the total pore volumes do not vary with the Cr and Si contents. The ***n*CrSiAl** materials have significantly higher surface areas relative to their ***n*CrSiZr** counterparts.

Transmission electron microscopy (TEM) was employed to determine the morphology of the Cr/Si/M/O samples after calcination at 773 K under O_2. In all cases, the samples are composed of aggregates of primary particles (from 50 to $>$ 500 nm in diameter), and no crystalline domains are apparent.

The crystallization behavior of the xerogels was monitored as a function of calcination temperature by powder X-ray diffraction (PXRD). All of the ***n*CrSiZr** xerogels are amorphous after calcination at 873 K under O_2; however, after calcination at 1073 K crystalline ZrO_2 (tetragonal) is observed, as shown in Fig. 1a for **10CrSiZr**. For comparison, the as-synthesized (uncalcined) ZrO_2 xerogel exhibits PXRD reflections attributed to both monoclinic and tetragonal ZrO_2 crystallites (Fig. 1b).

No Cr_2O_3 domains are observed for the ***n*CrSiZr** xerogels after calcination at 1473 K (by PXRD), which suggests

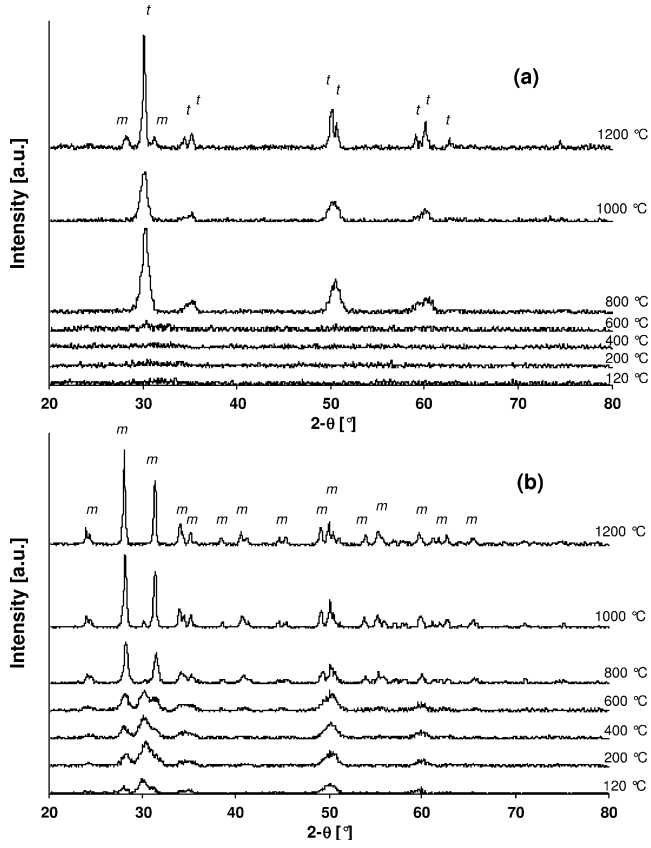

Fig. 1. Powder X-ray diffraction patterns at various calcination temperatures (under O_2) of: (a) **10CrSiZr** and (b) ZrO_2 from the thermolysis of $Zr[OCMe_2Et]_4$. *t*, tetragonal ZrO_2; *m*, monoclinic ZrO_2.

that the Cr species are well dispersed. The crystallization of Cr_2O_3 has been previously observed at 1173 K (by PXRD) for Cr/Zr/O samples of similar Cr contents (1–10 wt%) but prepared by aqueous impregnation methods [54]. The delay of crystallization to 1173 K was described as arising from well-dispersed surface Cr species. Therefore, the lack of Cr_2O_3 crystallization at calcination temperatures up to 1473 K in the ***n*CrSiZr** samples described here suggests that the initially formed Cr species are dispersed to an even greater degree. Similarly, all of the ***n*CrSiAl** xerogels are amorphous in their as-synthesized state, and they remain

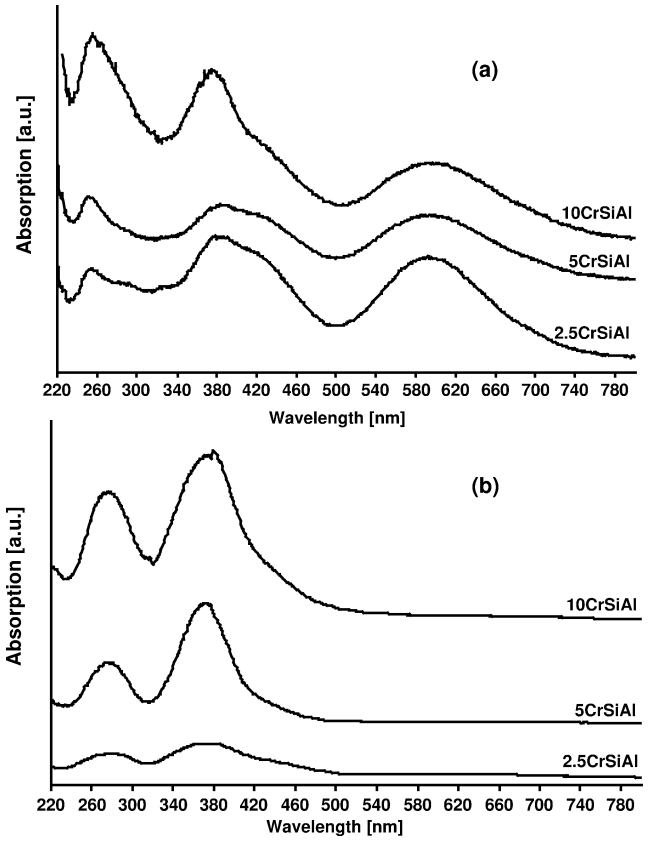

Fig. 2. Diffuse reflectance UV–vis spectra of **2.5CrSiAl**, **5CrSiAl**, and **10CrSiAl**: (a) as-synthesized and (b) after calcination at 773 K under O_2 for 2 h.

amorphous after calcination at 1473 K for 2 h (i.e., no Cr_2O_3 or Al_2O_3 domains are observed). This suggests that the Cr species are also highly dispersed within these materials. The high degree of homogeneity in the materials described here can be attributed, at least in part, to use of the TMP approach for their syntheses.

Thermogravimetric analyses (TGA) of the as-synthesized xerogels, under calcination conditions (O_2, 10 K min^{-1}), reveal 10 to 25% mass reductions below 873 K attributed to loss of H_2O (physisorbed and chemisorbed) and trace residual organics. At temperatures greater than ca. 873 K, no additional mass loss is observed. Differential scanning calorimetry (DSC) studies of the ***n*CrSiZr** and pure ZrO_2 samples under calcination conditions (O_2, heated at 10 K min^{-1}) do not reveal any exothermic transitions (for crystallization), and this suggests that the crystallization of ZrO_2 is slow under these conditions [18,54,55]. Interestingly, the DSC trace for **10CrSiAl** reveals a single small exotherm centered at 1333 K, attributed to mullite ($3Al_2O_3 \cdot 2SiO_2$) crystallization from a highly homogeneous aluminosilicate sample [25]. The apparent mullite domains were not detected by PXRD, presumably due to their small size and the relatively small amount of Si present in the sample. No DSC transitions are observed for **2.5CrSiAl** or **5CrSiAl**.

Diffuse-reflectance UV–vis (DRUV–vis) spectroscopy of the as-synthesized and calcined materials (773 K, O_2) was used to provide insight into the nature of the Cr species in these materials. Previous DRUV–vis studies by Weckhuysen and co-workers on the nature of Cr centers on various support materials revealed four types of species [56–60]. Monochromate species exhibit absorption bands at ca. 275 and 370 nm; dichromate and polychromate species (indistinguishable) give rise to bands at ca. 275, 320, and 445 nm; pseudooctahedral Cr^{3+} species appear at ca. 295, 465, and 625 nm; and bands for pseudooctahedral Cr^{2+} species are at ca. 800 nm [58]. As shown in Fig. 2a, the as-synthesized (uncalcined) ***n*CrSiAl** samples all exhibit DRUV–vis spectra with broad bands (centered at ca. 255, 380, and 435 nm) characteristic of a ligand-to-metal charge transfer (LMCT) from O^{2-} to Cr^{6+} in mono, di-, and polychromates. Significantly, an intense band at ca. 595 nm suggests that most of the chromium in these samples exists as octahedral Cr^{3+}, especially given that d–d transitions are considerably weaker than LMCT bands [56–60]. After calcination at 773 K under O_2, the DRUV–vis spectra of these ***n*CrSiAl** materials exhibit intense bands at ca. 275 and 375 nm with a shoulder at ca. 440 nm. This suggests the presence of only monochromate species, with smaller amounts of di- and polychromates. Although the presence of small quantities of Cr^{3+} species cannot be excluded, the DRUV–vis spectra of the samples after calcination at 773 K do not indicate the presence of such species (Fig. 2b). Similar behavior has been observed for related chromium-containing oxide materials with similar Cr contents [33,56–60].

The DRUV–vis spectra of the uncalcined (as-synthesized) ***n*CrSiZr** materials all contain a major band at ca. 270 nm with a broad shoulder extending out to 500 nm, indicative of various chromate species (Fig. 3a). A small band at ca. 615 nm, attributed to Cr^{3+} species, is also observed for these samples. The DRUV–vis spectra of the calcined ***n*CrSiZr** materials (773 K, O_2) exhibit features consistent with the presence of chromate species, and no Cr^{3+} species were detected (Fig. 3b). Qualitatively, the color changes associated with calcination of the samples are consistent with the DRUV–vis spectra, in that the green color of the as-synthesized materials suggests the presence of Cr^{3+} species, and the color change to yellow upon calcination at 773 K is consistent with oxidation to Cr^{6+} [57]. The initial presence of significant amounts of Cr^{3+} species suggests that the chemistry involved in the transformation to the solid material primarily involves a Cr^{4+} to Cr^{3+} reduction. The apparently large amounts of monochromate species (vs di- and polychromates) for the ***n*CrSiAl** and ***n*CrSiZr** materials after calcination at 773 K suggest that the samples contain well-dispersed chromium species. The ability of Al_2O_3 and ZrO_2 to stabilize dispersed chromate species upon calcination under O_2 at moderate temperatures is well documented [56–60].

To further probe the nature of the chromium centers in the materials described here, chromium X-ray absorption near-

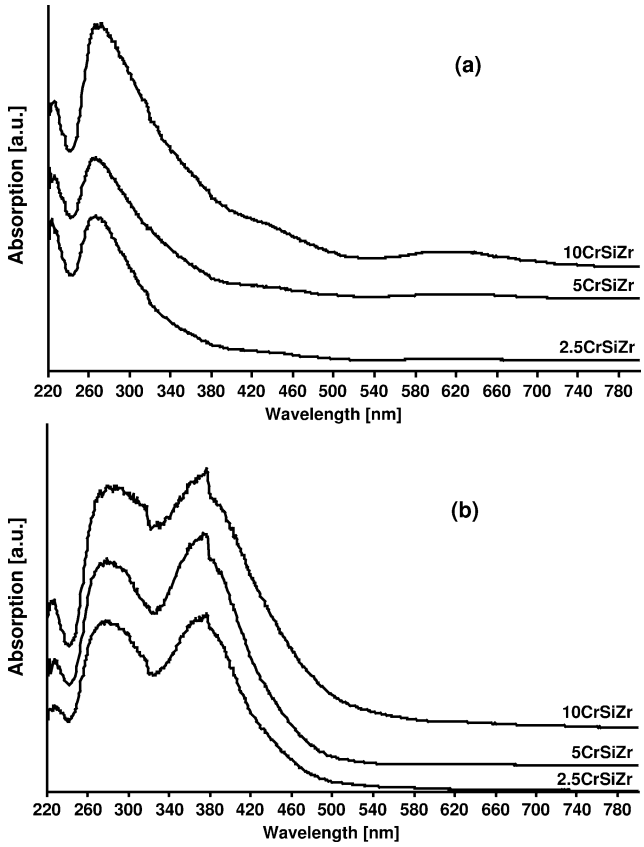

Fig. 3. Diffuse reflectance UV–vis spectra of **2.5CrSiZr**, **5CrSiZr**, and **10CrSiZr**: (a) as-synthesized and (b) after calcination at 773 K under O_2 for 2 h.

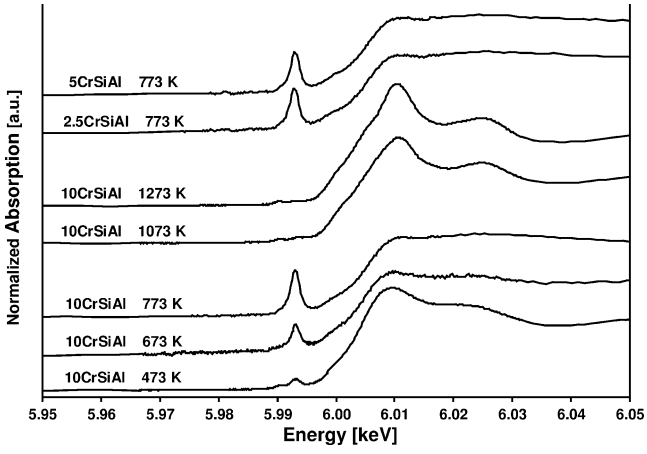

Fig. 4. XANES spectra at the Cr *K*-edge of **10CrSiAl** (calcined at 473, 673, 773, 1273, and 1473 K under O_2), and **2.5CrSiAl** and **5CrSiAl** calcined at 773 K under O_2.

edge structure (XANES) studies of the ***n*CrSiAl** samples were performed (Fig. 4). XANES spectra were also acquired for Cr_2O_3, $CrCl_2$, $Cr(O^tBu)_4$, $(^tBuO)_3CrOSi(O^tBu)_3$, CrO_3, K_2CrO_4, and $K_2Cr_2O_7$ as reference materials (Fig. 5). The nature of the preedge feature in Cr *K*-edge XANES measurements is indicative of specific coordination geometries, with tetrahedral environments giving rise to intense

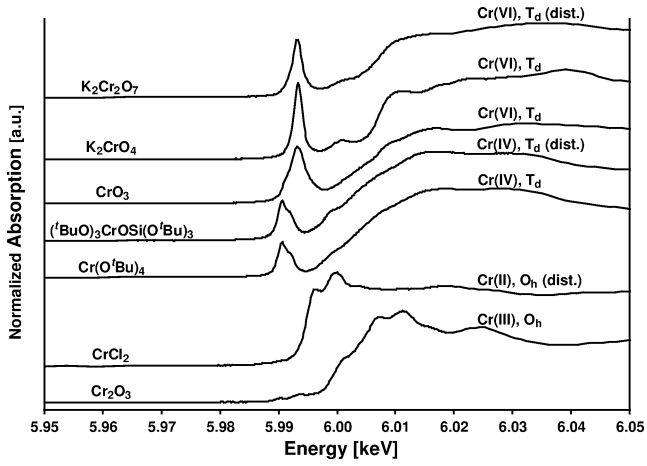

Fig. 5. XANES spectra at the Cr *K*-edge of various reference materials.

peaks and octahedral species providing very weak peaks, or none at all [61,62]. XANES analyses of **10CrSiAl** after calcination at 473, 673, and 773 K reveal the presence of increasing amounts of tetrahedral Cr^{6+} species, as indicated by the presence of a preedge feature that closely resembles that for the tetrahedral Cr^{6+} references (Figs. 4 and 5). No absorptions can be attributed to the presence of tetrahedral Cr^{4+} or distorted octahedral Cr^{2+} species for the **10CrSiAl** samples. Octahedral Cr^{3+} species are not readily detected by XANES measurements (see Cr_2O_3 in Fig. 5) [61]; however DRUV–vis spectroscopy revealed the presence of such components as the dominant species in **10CrSiAl** after calcination at 473 K (but not 673 or 773 K). XANES spectra of **10CrSiAl** after calcination at 1273 and 1473 K do not exhibit a preedge feature and closely resemble the spectrum for pure Cr_2O_3. This suggests that the Cr species in these samples are predominantly octahedral Cr^{3+} in small Cr_2O_3 domains (undetected by PXRD). Chromium XANES spectra of **2.5CrSiAl** and **5CrSiAl** after calcination at 773 K are similar to that for **10CrSiAl** after calcination at 773 K, in that they exhibit significant amounts of tetrahedral Cr^{6+} species (Fig. 4).

The first derivative of the XANES spectrum can be used to identify the position of the main absorption edge, and the correlation of this edge energy with the oxidation state of Cr species has been previously reported [61]. It has been observed that chromium species with higher oxidation states exhibit absorption edges at higher energy [61]. Similar analyses of the XANES data reported here have provided energies for the main absorption edges of the reference materials and the ***n*CrSiAl** samples (Table 2).

3.3. Oxidative dehydrogenation of propane

We have previously observed that propane ODH catalysts prepared by the TMP method exhibit improved performance relative to catalysts of the same composition but generated by aqueous impregnation techniques [20,23,29,30,63]. We therefore investigated the ***n*CrSiAl** and ***n*CrSiZr** materials

Table 2
XANES data for Cr reference materials, **2.5CrSiAl**, **5CrSiAl**, and **10CrSiAl**

Sample/calcination temperature	Main edge energy (keV)	Cr oxidation state	Cr geometry
$CrCl_2$	5.9982	(II)	Dist. O_h
Cr_2O_3	6.0033	(III)	O_h
$Cr(O^tBu)_4$	6.0029	(IV)	T_d
$(^tBuO)_3CrOSi(O^tBu)_3$	6.0031	(IV)	Dist. T_d
CrO_3	6.0071	(VI)	T_d
K_2CrO_4	6.0068	(VI)	T_d
$K_2Cr_2O_7$	6.0074	(VI)	Dist. T_d
10CrSiAl/473 K	6.0042		
10CrSiAl/673 K	6.0048		
10CrSiAl/773 K	6.0057		
10CrSiAl/1273 K	6.0038		
10CrSiAl/1473 K	6.0034		
2.5CrSiAl/773 K	6.0054		
5CrSiAl/773 K	6.0058		

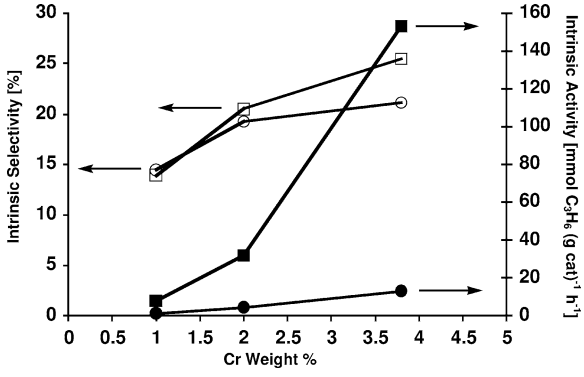

Fig. 6. Intrinsic selectivities and activities of the ***n*CrSiZr** catalysts plotted versus Cr content for the oxidative dehydrogenation of propane at 606 (circles) and 673 K (squares).

as catalysts for propane ODH. The ODH reactions were run in a fixed-bed flow reactor using a large excess of propane in the feed. The catalysts were calcined at 773 K under an atmosphere of He/O_2 ($\sim 10/1$) for a minimum of 2 h prior to reaction. Data corresponding to low propane conversions were collected to allow for the accurate determination of intrinsic activities and selectivities by extrapolation to infinite flow rate and 0% conversion, respectively. Bell, Iglesia, and co-workers have shown that this method for analyzing catalytic data is useful for comparing ODH catalyst performances [50,51]. Figs. 6 and 7 display plots of the intrinsic propylene selectivity (%) and the activity for propylene formation (mmol propylene $g_{cat}^{-1}\,h^{-1}$) as a function of Cr content, for ODH reactions run at 606 and 673 K using the ***n*CrSiZr** (Fig. 6) and ***n*CrSiAl** (Fig. 7) catalysts. It is apparent that the intrinsic selectivity for propylene is low in all cases ($< 30\%$) and that the ODH activity is significantly higher for the ***n*CrSiZr** catalysts (Table 3). The high activity in the ***n*CrSiZr** catalysts presumably results from the crystalline nature of the ZrO_2 support, which drives more Cr species to the surface rendering them accessible for reaction [30]. Despite their higher surface areas, the amorphous

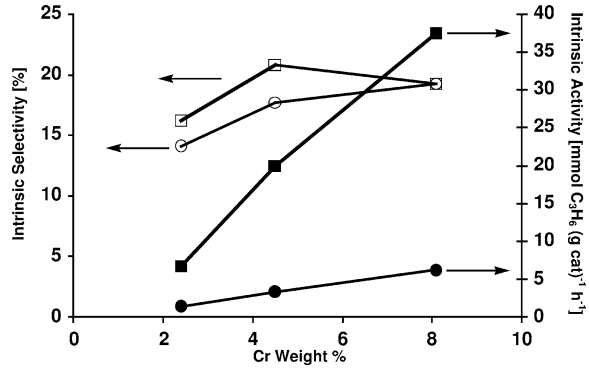

Fig. 7. Intrinsic selectivities and activities of the ***n*CrSiAl** catalysts plotted versus Cr content for the oxidative dehydrogenation of propane at 606 (circles) and 673 K (squares).

nature and higher thermal stability of the ***n*CrSiAl** catalysts suggest that more Cr is present in the bulk and is not available for reaction, thus giving rise to lower activities when compared to their ***n*CrSiZr** counterparts. The activity of **10CrSiZr** at 673 K is among the highest values reported for an ODH catalyst, despite its poor selectivity [29,30,50,51]. For all of the ***n*CrSiZr** and ***n*CrSiAl** catalysts, activities increase with chromium content (Table 3). For comparison, previously reported Cr/Al_2O_3 catalysts prepared by wet impregnation (5–20 wt% Cr and 2–10 Cr nm^{-2}) exhibit good selectivities (from ca. 60–85%) with moderate activities (from 4.3 to 11.5 mmol propane converted $g_{cat}^{-1}\,h^{-1}$) at 673 K with propane conversions from 2 to 6% [33]. Previously reported, TMP-derived $V/Zr/O$ catalysts exhibit activities near 100 mmol propylene produced $g_{cat}^{-1}\,h^{-1}$ with intrinsic C_3H_6 selectivities approaching 90% at 673 K [30].

It has been shown that propane reacts with oxygen in parallel and sequential steps over metal oxide catalysts (Scheme 1) [50,51]. At low oxygen conversions, pseudo-first-order rate coefficients for the propane ODH step (k_1), the combustion of propane (k_2), and the combustion of propylene (k_3) can be obtained [50,51]. Kinetic analyses of the propane ODH reactions at 606 K using the ***n*CrSiAl** and ***n*CrSiZr** catalysts were performed (Table 4) according to the procedures outlined by Iglesia, Bell, and co-workers [50,51]. These studies reveal that the ***n*CrSiZr** catalysts exhibit k_2/k_1 ratios (the rate of propane combustion versus propane ODH) that decrease with increasing Cr content. Interestingly, the rates of propane ODH (k_1) and propane combustion (k_2) both increase with increasing Cr content; however, a greater increase in k_1 suggests that higher Cr contents are beneficial (Table 4). Additionally, analysis of the k_3/k_1 ratios for the ***n*CrSiZr** catalysts (the rate of propylene combustion versus propane ODH) shows that lower values are obtained for higher Cr contents. These kinetic analyses show that the rate of propylene combustion (k_3) is lower for higher Cr contents. Among the ***n*CrSiAl** catalysts, **5CrSiAl** exhibits the lowest k_2/k_1 and highest k_3/k_1 ratios, suggesting that effects other than Cr dispersion (i.e., the nature of active sites) are also important in these systems [33].

Table 3
Summary of the propane ODH reactions using the Cr xerogels

Catalyst	Mass (mg)	T (K)	Intrinsic activity[a]	Intrinsic selectivity[b]	Intrinsic TOF[c]	Activity[d]	Selectivity[e]	TOF[f]	CO_2/CO ratio[g]
2.5CrSiAl	32	606	2.6	16.2	5.7	2.2	15.9	4.7	3.1
		673	12.6	14.1	27.4	6.6	11.7	14.4	2.2
5CrSiAl	10	606	3.2	20.8	3.7	2.0	13.6	2.3	4.0
		673	19.9	17.7	23.0	6.9	12.6	8.0	2.8
10CrSiAl	15	606	5.2	19.3	3.4	4.4	17.5	2.8	4.3
		673	37.5	19.3	24.2	19.0	15.8	12.3	3.0
2.5CrSiZr	18	606	1.1	14.5	5.6	0.9	11.4	4.3	3.2
		673	7.9	13.9	40.0	3.9	9.4	19.8	2.8
5CrSiZr	18	606	4.1	19.3	10.7	3.5	17.4	9.1	5.5
		673	31.7	20.5	82.5	16.2	14.6	42.2	4.5
10CrSiZr	10	606	11.9	21.1	16.3	10.6	19.8	14.5	7.3
		673	153.2	25.5	209.8	64.2	18.3	87.9	6.1

[a] Millimoles of C_3H_6 produced $g_{cat}^{-1}\,h^{-1}$ at 0% conversion.
[b] Selectivity (%) for C_3H_6 production at 0% conversion.
[c] Moles of C_3H_6 produced $mol_{Cr}^{-1}\,h^{-1}$ at 0% conversion.
[d] Millimoles of C_3H_6 produced $g_{cat}^{-1}\,h^{-1}$ at 0.5% (606 K) or 5% (673 K) C_3H_8 conversion.
[e] Selectivity (%) for C_3H_6 production at 0.5% (606 K) or 5% (673 K) C_3H_8 conversion.
[f] Moles of C_3H_6 produced $mol_{Cr}^{-1}\,h^{-1}$ at 0.5% (606 K) or 5% (673 K) C_3H_6 conversion.
[g] Ratio of CO_2/CO for the reaction at the lowest flow rate; the ratio was similar at higher total flow.

Table 4
Kinetic analyses of propane ODH reactions using ***n*CrSiAl** and ***n*CrSiZr** at 606 K

Catalyst	k_1 ($L\,mol^{-1}\,s^{-1}$)	k_2 ($L\,mol^{-1}\,s^{-1}$)	k_3 ($L\,mol^{-1}\,s^{-1}$)	k_2/k_1	k_3/k_1
2.5CrSiAl	0.17	0.93	40.2	5.48	237
5CrSiAl	0.22	0.85	72.9	3.89	333
10CrSiAl	0.21	0.89	22.2	4.32	108
2.5CrSiZr	0.36	2.09	203	5.80	562
5CrSiZr	0.64	2.73	110	4.31	173
10CrSiZr	0.92	3.53	69.0	3.85	75.1

The higher propylene selectivities for the recently reported Cr/Al_2O_3 catalysts prepared by wet impregnation [33], compared to the catalysts described here, appear to result from the presence of highly active combustion sites in the ***n*CrSiAl** and ***n*CrSiZr** catalysts. These sites may result from the highly dispersed nature of the Cr in these high surface area materials. Indeed, polymeric Cr oxides are thought to be responsible for the ODH reaction, and the selectivity for propylene increases with increasing Cr content for Cr/Al_2O_3 catalysts [33]. Also, studies of propane ODH reactions using Cr/Si/O materials produced from **1** via TMP methods revealed improved performance for less homogeneous materials that contained more polymeric Cr oxide species [23]. For Cr/Al_2O_3 catalysts obtained via wet impregnation, it was suggested that a decrease in the k_2/k_1 ratio is not responsible for the increased propylene selectivity with increasing Cr loading [33]. Similarly for the catalysts described here, the k_2/k_1 ratios for the materials within each ***n*CrSiAl** and ***n*CrSiZr** set are similar. In contrast, the k_3/k_1 ratios of the catalysts within each ***n*CrSiAl** and ***n*CrSiZr** set are quite different, suggesting that the key difference between catalysts with different Cr loadings is their activities for propylene oxidation. The 1/1 Si/Cr ratio in the ***n*CrSiAl** and ***n*CrSiZr** catalysts may be problematic, as Si is known to negatively impact the propylene selectivity for vanadium-based ODH catalysts due to the presence of Brønsted acid sites [29,30]. All of these results support the notion that more efficient propane ODH catalysts should be based on Cr/M/O materials with high Cr loadings and polymeric CrO_x species as the active sites.

3.4. Dehydrogenation of propane

The excellent performance of Cr-based oxides as catalysts for the dehydrogenation of propane prompted us to study the ***n*CrSiAl** and ***n*CrSiZr** materials in this context [32–47]. These DH reactions were run in a fixed-bed flow reactor with moderate propane concentrations (1–6 mol%) and propane conversions ranging from ~ 0.5 to 38%. The catalysts were calcined at 773 K under an atmosphere of He/O_2 ($\sim 10/1$) for 2 h, and subsequently under He for an additional 2 h prior to reaction. Propane conversions and product amounts were monitored for an extended period at constant residence times and reaction temperatures. Table 5 gives the results of catalytic propane DH reactions at 723 K and low propane conversions. Overall, the ***n*CrSiZr** catalysts outperformed their ***n*CrSiAl** counterparts in terms of activity, with all catalysts exhibiting ca. 100% selectivity for propylene formation. Deactivation of the catalysts, attributed to coking, was observed with increasing time on-line [32]. However, heating the catalysts at 773 K (under He/O_2 for 2 h and He for 1 h) after a catalytic run led to full regeneration of the activity for all catalysts (3 cycles). On a per gram basis, the activities (mmol $C_3H_6\,g_{cat}^{-1}\,h^{-1}$) of the ***n*CrSiAl** catalysts increased with increasing Cr wt%; however **2.5CrSiAl** is the most active when activities are considered on a per mole Cr basis (mol C_3H_6 mol $Cr^{-1}\,h^{-1}$). For the ***n*CrSiZr** catalysts, activities on a per gram or a per mole Cr basis increased with

Table 5
Propane DH reactions using the Cr xerogels at 723 K and low C_3H_8 conversions

Catalyst	Mass (mg)	mol% C_3H_8	Res. time (s)	Conversion (%)[a]			Selectivity (%)[b]				Activity[c]		TOF[d]	
							C_3H_6		CH_4					
				t_1	t_2	t_3	t_1	t_3	t_1	t_3	t_1	t_3	t_1	t_3
2.5CrSiAl	70	5.5	0.67	0.59	0.38	0.32	100	100	0	0	0.37	0.20	0.81	0.44
5CrSiAl	50	5.5	0.61	0.48	0.30	0.26	100	100	0	0	0.38	0.23	0.44	0.27
10CrSiAl	20	5.5	0.66	0.24	0.21	0.18	100	100	0	0	0.53	0.35	0.35	0.25
2.5CrSiZr	50	5.1	0.69	3.02	2.75	2.70	98.5	99.5	0.8	0.6	2.43	2.17	12.30	11.02
5CrSiZr	50	5.1	0.68	1.93	1.88	1.82	100	100	0	0	1.58	1.49	4.11	3.88
10CrSiZr	30	5.5	0.68	0.70	0.61	0.46	100	100	0	0	1.02	0.66	1.40	0.90

[a] Conversion of C_3H_8 at $t_1 = 35$ min, $t_2 = 105$ min, and $t_3 = 170$ min (***n*CrSiAl**) or 400 min (***n*CrSiZr**).
[b] Selectivity at $t_1 = 35$ min and $t_3 = 170$ min (***n*CrSiAl**) or 400 min (***n*CrSiZr**). C_2H_4 and C_2H_6 were not observed.
[c] Millimoles of C_3H_6 produced $g_{cat}^{-1}\,h^{-1}$.
[d] Moles of C_3H_6 produced $mol_{Cr}^{-1}\,h^{-1}$ at $t_1 = 35$ min and $t_3 = 105$ min (***n*CrSiAl**) or 400 min (***n*CrSiZr**).

Table 6
Propane DH reactions using **2.5CrSiZr** at 723 or 763 K and high C_3H_8 conversions

Catalyst	Mass (mg)	mol% C_3H_8	Res. time (s)	Conversion (%)[a]			Selectivity (%)[b]						Activity[c]		TOF[d]	
							C_3H_6		CH_4		C_2					
				t_1	t_2	t_3	t_2	t_3	t_2	t_3	t_2	t_3	t_1	t_3	t_1	t_3
2.5CrSiZr	50	5.1	0.69	3.02	2.75	2.70	98.5	99.4	0.8	0.6	0.0	0.0	2.4	2.2	12.3	11.0
2.5CrSiZr	130	2.9	0.9	14.5	16.6	13.0	96.4	97.3	1.9	1.4	0.7	0.5	1.9	1.7	9.4	8.6
2.5CrSiZr	130	1.6	0.88	20.2	20.4	16.3	95.1	96.8	2.6	1.8	0.6	0.3	1.5	1.2	7.5	6.2
2.5CrSiZr[e]	130	2.9	1.1	31.9	22.3	8.40	95.2	96.1	2.4	1.8	1.1	0.3	3.2	0.9	16.4	4.5
2.5CrSiZr	260	1.9	1.02	37.8	34.3	22.7	91.1	94.7	4.1	2.2	2.8	1.9	1.3	0.8	6.5	4.2
2.5CrSiZr[f]	260	1.7	1	33.8	31.5	20.0	91.6	95.3	3.7	1.9	3.0	2.1	1.1	0.7	5.3	3.4

[a] Conversion of C_3H_8 at $t_1 = 35$ min, $t_2 = 105$ min, and $t_3 = 400$ min.
[b] Selectivity at $t_2 = 105$ min and $t_3 = 400$ min. C_2 represents the sum of C_2H_4 and C_2H_6 (usually 2/1 C_2H_4/C_2H_6).
[c] Millimoles C_3H_6 produced $g_{cat}^{-1}\,h^{-1}$ at $t_1 = 35$ min and $t_3 = 400$ min.
[d] Moles of C_3H_6 produced $mol_{Cr}^{-1}\,h^{-1}$ at $t_1 = 35$ min and $t_3 = 400$ min.
[e] Reaction at 763 K.
[f] Using regenerated catalyst from the above reaction.

decreasing Cr content. Given that agglomerated species are more likely to exist at higher Cr loadings, the activity data for both the ***n*CrSiAl** and ***n*CrSiZr** catalysts imply that isolated sites are more active for the DH reaction. These results are consistent with published reports on Cr-based DH catalysts, for which activity levels off or decreases at higher Cr loadings (4 to 10 wt%) [32]. It has been previously observed that, in addition to the reversible coking process, slight irreversible deactivation occurs for Cr/Al/O catalysts with increasing time on-line and through regeneration cycles; however, consistent performance can be obtained by gradually increasing the reaction temperature [32]. This gradual, irreversible deactivation of Cr/Al_2O_3 catalysts has been attributed to the incorporation of Cr^{3+} species into vacant Al^{3+} sites in the Al_2O_3 support [32]. For Cr/Al_2O_3 catalysts, it has been shown that coordinatively unsaturated and isolated Cr^{3+} species are formed under typical propane DH conditions (upon reduction of Cr^{6+} species), and that these species are active sites [32,45]. Additionally, Cr^{3+} species in small amorphous clusters have been proposed as active DH sites [32].

At low propane conversions, **2.5CrSiZr** is by far the most active catalyst on a per gram or per mole Cr basis (Table 5). Thus, we elected to study propane DH reactions with **2.5CrSiZr** under conditions that resulted in higher conversions, to more accurately represent those required for industrial application (Table 6, Figs. 8 and 9). Use of larger amounts of **2.5CrSiZr** under various concentrations of propane and different residence times led to propane conversions that were greater than 35%, with propylene selectivities exceeding 90%. To monitor catalyst performance over an extended period, the catalytic runs were executed over the course of ca. 7 h with GC samples taken approximately every 18 min. Only moderate deactivation due to coke formation was observed for **2.5CrSiZr** at 723 K, with higher propane conversions giving rise to greater deactivation. Calcination of the catalysts at 773 K under O_2 leads to coke removal and regeneration of the catalyst. For example, after a 7-h catalytic run at very high conversions (up to 35%), a **2.5CrSiZr** catalyst was treated at 773 K under He/O_2 for 3 h with a subsequent He treatment for 1 h. Exposure of this regenerated catalyst to propane led to activity and selectivity values that were nearly identical to those of a previous run when the (small) differences in the conditions are considered (Table 6, Figs. 8 and 9). Regeneration times greater than 3 h may be required to bring the catalyst back to full

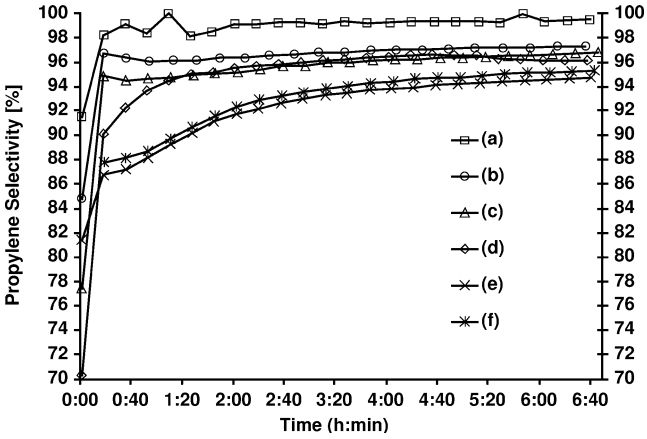

Fig. 8. Propylene selectivity plotted versus time for propane DH using **2.5CrSiZr** under various conditions: (a) 50 mg of catalyst, 723 K, 5.1 mol% C_3H_8, and 0.69 s residence time; (b) 130 mg of catalyst, 723 K, 2.9 mol% C_3H_8, and 0.90 s residence time; (c) 130 mg of catalyst, 723 K, 1.6 mol% C_3H_8, and 0.88 s residence time; (d) 130 mg of catalyst, 763 K, 2.9 mol% C_3H_8, and 1.10 s residence time; (e) 260 mg of catalyst, 723 K, 1.9 mol% C_3H_8, and 1.02 s residence time; (f) 260 mg of catalyst regenerated from (e), 723 K, 1.7 mol% C_3H_8, and 1.00 s residence time.

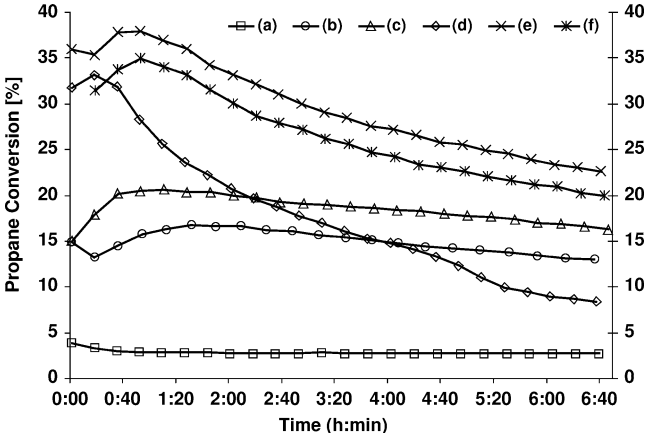

Fig. 9. Propane conversion plotted versus time for propane DH using **2.5CrSiZr** under various conditions: (a) 50 mg of catalyst, 723 K, 5.1 mol% C_3H_8, and 0.69 s residence time; (b) 130 mg of catalyst, 723 K, 2.9 mol% C_3H_8, and 0.90 s residence time; (c) 130 mg of catalyst, 723 K, 1.6 mol% C_3H_8, and 0.88 s residence time; (d) 130 mg of catalyst, 763 K, 2.9 mol% C_3H_8, and 1.10 s residence time; (e) 260 mg of catalyst, 723 K, 1.9 mol% C_3H_8, and 1.02 s residence time; (f) 260 mg of catalyst regenerated from (e), 723 K, 1.7 mol% C_3H_8, and 1.00 s residence time.

activity after longer catalytic runs. For the propane DH reaction performed at 763 K with **2.5CrSiZr**, initial conversion was very high with excellent propylene selectivity; however, the catalyst deactivated at a severe rate to levels below those observed for the reaction at 723 K (Table 5, Fig. 9). This appears to reflect a dramatic increase in the rate of coking at the higher temperature.

Although it is difficult to compare catalysts operating under different conditions, the excellent performance of **2.5CrSiZr** for propane DH at low temperatures suggests that the TMP cothermolysis method may offer improvements over the propane DH catalysts studied previously [32–47]. For example, a previously reported Cr/Al_2O_3 propane DH catalyst (9% Cr) operated at propane conversions from 26 to 28% with 68 to 76% propylene selectivities at 833 K after 100 min of reaction time [35]. Other Cr/Al_2O_3 catalysts are reported to have activities of 1.8 mmol C_3H_6 produced $g_{cat}^{-1}\,h^{-1}$ at 773 K after 100 min [43], or propane conversions ranging from 25 to 47% with propylene selectivities from 60 to 90% at 873 K [36,46]. Catalysts based on the Cr/SiO_2 system were generally less active (0.6 mmol C_3H_6 produced $g_{cat}^{-1}\,h^{-1}$ at 773 K after 100 min) [43]. Chromium-containing Zr/P/O catalysts exhibited activities from 0.4 to 8.4 mmol C_3H_6 produced $g_{cat}^{-1}\,h^{-1}$ with propylene selectivities from 79 to 94% at propane conversions from 2 to 18% at 823 K [38,39]. Finally, Cr/ZrO_2 catalysts appear to be the most active, with values ranging from 3.6 to 4.8 mmol C_3H_6 produced $g_{cat}^{-1}\,h^{-1}$ at 723 K [45]. At higher temperatures (823 K), these catalysts exhibited selectivities for propylene from 85 to 98% with propane conversions decreasing from an initial value of 54 to 19% after ca. 100 min [45].

Difficulties in obtaining high surface area and thermally stable zirconia supports were cited as being a large reason for limited use of Cr/ZrO_2 catalysts for large-scale propane DH reactions [45]. Use of the TMP-cothermolysis method has resulted in ***n*CrSiZr** materials with high surface areas after calcination at temperatures above those required for the propane DH reaction. The excellent selectivity and high activity of **2.5CrSiZr** as a propane DH catalyst, coupled with the low temperature required for its use, indicate that this catalyst is among the best known for this process.

4. Concluding remarks

High surface area, homogeneous xerogels of the types $Cr_xSi_xAl_yO_z$ (***n*CrSiAl**) and $Cr_xSi_xZr_yO_z$ (***n*CrSiZr**) are easily synthesized via cothermolyses under nonaqueous conditions using $(^tBuO)_3CrOSi(O^tBu)_3$ and $[Al(O^tBu)_3]_2$ or $Zr[OCMe_2Et]_4$. These materials have highly dispersed chromium centers after calcination at 773 K (by PXRD, DRUV–vis, TEM, and XANES). The chromium in the as-synthesized ***n*CrSiAl** samples is present as isolated octahedral Cr^{3+} species. Calcination of the ***n*CrSiAl** samples at moderate temperatures (673 and 773 K) under O_2 results in high conversion to tetrahedral Cr^{6+} species and no reduced species. Calcination at higher temperatures (1273 or 1473 K) under O_2 produces octahedral Cr^{3+} species, likely in the form of small (or amorphous) Cr_2O_3 domains. The ***n*CrSiZr** samples appear to have significant amounts of both Cr^{3+} and Cr^{6+} species in their as-synthesized state; however, calcination at 773 K leads to formation of only Cr^{6+} species.

The ***n*CrSiAl** and ***n*CrSiZr** catalysts are active for propane ODH, with **10CrSiZr** having an activity (based on propylene production) that is among the highest values reported for this reaction. Unfortunately, the selectivity toward propylene production is low for all catalysts examined. Ki-

netic analyses indicate that the poor selectivities arise from very high rates for propylene combustion (k_3). It appears that well-dispersed Cr species are not selective for propylene, and that polymeric chromium oxides are preferred [33]. For the ***n*CrSiZr** catalysts, an increase in the rate of propane ODH (k_1) and a decrease in the rate of propylene combustion (k_3) with increasing chromium content indicate that different sites are at least partially responsible for these reactions. Comparisons to previously reported Al_2O_3-supported Cr catalysts synthesized via wet impregnation reveal that the catalysts prepared here exhibit higher ODH activities, but lower selectivities for propylene formation [33]. In addition, comparisons of the Cr-based catalysts reported here with previously reported V/Zr/O ODH catalysts synthesized via thermolytic molecular precursor methods reveal that the catalysts have comparable activities, but that selectivities for propylene are superior for the vanadium-based species [30].

Propane DH reactions under mild conditions (723 K) using the ***n*CrSiAl** and ***n*CrSiZr** catalysts are characterized by high selectivities at low propane conversions. The ***n*CrSiZr** catalysts are generally more active than their ***n*CrSiAl** counterparts. Lower Cr contents give rise to higher activities on a per Cr basis, suggesting that isolated sites are preferred. Detailed investigations using **2.5CrSiZr** led to propane conversions greater than 35%, with propylene selectivities approaching 95%. These values are among the best reported for propane DH catalysts, particularly at such a low reaction temperature. Deactivation due to coking was observed over the course of the reactions; however, calcination under He/O_2 at 773 K was effective for regeneration of the catalysts. Therefore, for propane ODH, the best results seem to be associated with chromate clusters, whereas for propane DH, well-dispersed (and presumably isolated) chromium species are most effective.

Acknowledgments

We are grateful for the support of this work by the Office of Basic Energy Sciences, Chemical Sciences Division, of the US Department of Energy under Contract No. DE-AC03-76SF00098. We also thank Prof. A. Stacy for the use of instrumentation (PXRD, DRUV–vis), Dr. J. Male for assistance with the XANES studies, and the Stanford Synchrotron Radiation Laboratory (SSRL).

References

[1] J.-P. Jolivet, Metal Oxide Chemistry and Synthesis. From Solution to Solid State, Wiley, Chichester, 2000.
[2] C.K. Narula, Ceramic Precursor Technology and Its Applications, Dekker, New York, 1995.
[3] D.R. Uhlmann, D.R. Ulrich (Eds.), Ultrastructure Processing of Advanced Materials, Wiley, New York, 1992.
[4] C.J. Brinker, G.W. Scherer, Sol–Gel Science, Academic Press, Boston, 1990.
[5] A.H. Cowley, R.A. Jones, Angew. Chem. Int. Ed. Engl. 28 (1989) 1208.
[6] F. Chaput, A. Lecomte, A. Dauger, J.P. Boilot, Chem. Mater. 1 (1989) 199.
[7] A.W. Apblett, A.C. Warren, A.R. Barron, Chem. Mater. 4 (1992) 167.
[8] C.D. Chandler, C. Roger, M.J. Hampden-Smith, Chem. Rev. 93 (1993) 1205.
[9] A. Stein, S.W. Keller, T.E. Mallouk, Science 259 (1993) 1558.
[10] D.C. Bradley, Polyhedron 13 (1994) 1111.
[11] U. Schubert, N. Hüsing, A. Lorenz, Chem. Mater. 7 (1995) 2010.
[12] D.B. Amabilino, J.F. Stoddart, Chem. Rev. 95 (1995) 2725.
[13] C.L. Bowes, G.A. Ozin, Adv. Mater. 8 (1996) 13.
[14] U. Schubert, J. Chem. Soc., Dalton Trans. (1996) 3343.
[15] K.W. Terry, C.G. Lugmair, P.K. Gantzel, T.D. Tilley, Chem. Mater. 8 (1996) 274.
[16] K. Su, T.D. Tilley, M.J. Sailor, J. Am. Chem. Soc. 118 (1996) 3459.
[17] K. Su, T.D. Tilley, Chem. Mater. 9 (1997) 588.
[18] K.W. Terry, C.G. Lugmair, T.D. Tilley, J. Am. Chem. Soc. 119 (1997) 9745.
[19] K.W. Terry, K. Su, T.D. Tilley, A.L. Rheingold, Polyhedron 17 (1998) 891.
[20] R. Rulkens, J.L. Male, K.W. Terry, B. Olthof, A. Khodakov, A.T. Bell, E. Iglesia, T.D. Tilley, Chem. Mater. 11 (1999) 2966.
[21] J.W. Kriesel, M.S. Sander, T.D. Tilley, Mater. Chem. 13 (2001) 3554.
[22] J.W. Kriesel, T.D. Tilley, J. Mater. Chem. 11 (2001) 1081.
[23] K.L. Fujdala, T.D. Tilley, Chem. Mater. 13 (2001) 1817.
[24] K.L. Fujdala, T.D. Tilley, J. Am. Chem. Soc. 123 (2001) 10133.
[25] C.G. Lugmair, K.L. Fujdala, T.D. Tilley, Chem. Mater. 14 (2002) 888.
[26] K.L. Fujdala, T.D. Tilley, Chem. Mater. 14 (2002) 1376.
[27] M. Jansen, E. Guenther, Chem. Mater. 7 (1995) 2110.
[28] A. Vioux, Chem. Mater. 9 (1997) 2292.
[29] R. Rulkens, T.D. Tilley, J. Am. Chem. Soc. 120 (1998) 9959.
[30] J.L. Male, H.G. Niessen, A.T. Bell, T.D. Tilley, J. Catal. 194 (2000) 431.
[31] H.H. Kung, Adv. Catal. 40 (1995) 1.
[32] B.M. Weckhuysen, R.A. Schoonheydt, Catal. Today 51 (1999) 223, and references therein.
[33] M. Cherian, M.S. Rao, W.-T. Yang, J.-M. Jehng, A.M. Hirt, G. Deo, Appl. Catal. A 233 (2002) 21.
[34] J. Sloczynski, B. Grzybowska, R. Grabowski, A. Kozlowska, K. Wcislo, Phys. Chem. Chem. Phys. 1 (1999) 333.
[35] L.R. Mentasty, O.F. Gorriz, L.E. Cadus, Ind. Eng. Chem. Res. 38 (1999) 396.
[36] O.F. Gorriz, L.E. Cadús, Appl. Catal. A 180 (1999) 247.
[37] F.E. Frey, W.F. Huppke, Ind. Eng. Chem. 25 (1933) 54.
[38] M. Alcántara-Rodríguez, E. Rodríguez-Castellón, A. Jiménez-López, Langmuir 15 (1999) 1115.
[39] F.J. Pérez-Reina, E. Rodríguez-Castellón, A. Jiménez-López, Langmuir 15 (1999) 8421.
[40] W.C. Chang, N. Mimura, M. Saito, I. Takahara, Catal. Today 45 (1998) 55.
[41] V. Indovina, Catal. Today 41 (1998) 95.
[42] S. De Rossi, M.P. Casaletto, G. Ferraris, A. Cimino, G. Minelli, Appl. Catal. A 167 (1998) 257.
[43] S. De Rossi, G. Ferraris, S. Fremiotti, E. Garrone, G. Ghiotti, M.C. Campa, V. Indovina, J. Catal. 148 (1994) 36.
[44] S. De Rossi, G. Ferraris, S. Fremiotti, V. Indovina, A. Cimino, Appl. Catal. A 106 (1993) 125.
[45] S. De Rossi, G. Ferraris, S. Fremiotti, A. Cimino, V. Indovina, Appl. Catal. A 81 (1992) 113.
[46] O.F. Gorriz, V.C. Corberán, J.L.G. Fierro, Ind. Eng. Chem. Res. 31 (1992) 2670.
[47] D. Sanfilippo, F. Buonomo, G. Fusco, M. Lupieri, I. Miracca, Chem. Eng. Sci. 47 (1992) 2313.
[48] T. Blasco, J.M. López Nieto, Appl. Catal. A 157 (1997) 117.
[49] S. Albonetti, F. Cavani, F. Trifirò, Catal. Rev. Sci. Eng. 38 (1996) 413.
[50] A. Khodakov, B. Olaf, A.T. Bell, E. Iglesia, J. Catal. 181 (1999) 205.

[51] A. Khodakov, J. Yang, S. Su, E. Iglesia, A.T. Bell, J. Catal. 177 (1998) 343.
[52] S. Brunauer, P.H. Emmett, E. Teller, J. Am. Chem. Soc. 60 (1938) 309.
[53] E.P. Barrett, L.G. Joyner, P.P. Halenda, J. Am. Chem. Soc. 73 (1951) 373.
[54] J.R. Sohn, S.G. Ryu, Langmuir 9 (1993) 126.
[55] M. Yashima, M. Kakihana, M. Yoshimura, Solid State Ionics 86 (1996) 1131.
[56] B.M. Weckhuysen, I.E. Wachs, R.A. Schoonheydt, Chem. Rev. 96 (1996) 3327.
[57] B.M. Weckhuysen, R.A. Schoonheydt, Catal. Today 49 (1999) 441.
[58] B.M. Weckhuysen, A.A. Verberckmoes, A.R. De Baets, R. Schoonheydt, J. Catal. 166 (1997) 160.
[59] B.M. Weckhuysen, A.A. Verberckmoes, A.L. Buttiens, A.R. Schoonheydt, J. Phys. Chem. 98 (1994) 579.
[60] B.M. Weckhuysen, L.M. De Ridder, R.A. Schoonheydt, J. Phys. Chem. 97 (1993) 4756.
[61] P.S. Devi, H.D. Gafney, V. Petricevic, R.R. Alfano, D. He, K.E. Miyano, Chem. Mater. 12 (2000) 1378.
[62] F. Rey, G. Sankar, T. Maschmeyer, J.M. Thomas, R.G. Bell, Top. Catal. 3 (1996) 121.
[63] C. Pak, A.T. Bell, T.D. Tilley, J. Catal. 206 (2002) 49.